THE
PHYSICAL REVIEW

A journal of experimental and theoretical physics established by E. L. Nichols in 1893

SECOND SERIES, VOL. 129, NO. 2 15 JANUARY 1963

Measurements of Electronic Thermal Conductivity in Magnetoplasmas*

F. ROSTAS, ASHOK K. BHATTACHARYA, AND J. H. CAHN
University of Illinois, Urbana, Illinois
(Received 1 March 1962)

Electronic thermal conduction in a magnetoplasma with electron number densities of the order of 10^{11} to 10^{12} cm^{-3}, where Coulomb interactions predominate, has been studied experimentally in neon discharges at a pressure of the order of 5 mm Hg, and magnetic fields up to 1200 Oe. The temperature distribution resulting from a very localized heating of the electron gas by an electromagnetic wave of frequency 7500 Mc/sec has been measured in a plane perpendicular to the magnetic field and at variable distances from the heated volume. The experimental results are compared with the predictions of Landshoff.

I. INTRODUCTION

THE theory of thermomagnetic effects including electron-electron interactions in a fully ionized gas has been in the literature for more than ten years.[1] Heretofore no experiment has been conducted to measure the electronic thermal transport coefficients of a magnetoplasma. The present paper reports results of experimental measurements of heat flow in the electron gas in an effectively fully ionized plasma placed in a magnetic field. The experimental measurements are compared with Landshoff's calculations.[1] This work is an extension of the earlier efforts to measure the electronic thermal conductivity of a plasma in the absence of an external magnetic field.[2,3]

It is interesting to note that an effectively fully ionized plasma can be simulated by a gaseous discharge in which the Coulomb interaction plays the dominant role. The most important criteria that an experimental measurement of electronic heat flow in an ionized medium be feasible, and that the results correspond to the fully ionized case are the following:

(1) The thermal relaxation length[2] in the electron gas should be long enough for accurate measurements of electronic temperature distribution to be made.

(2) The electron-ion interaction must dominate the electron-neutral interaction so that the plasma studied may simulate the fully ionized gas.

Thermal relaxation distance mentioned above in (1) arises from the heat equation,

$$\kappa\partial^2\theta/\partial x^2=\tfrac{3}{2}nk\theta/\tau_{ei},$$

in one dimension, where κ is the electron thermal conductivity, n is the electron number density, τ_{ei} is the electron-ion energy relaxation time,[4,5] and θ is the amount by which the electron temperature exceeds the ion temperature. Such an equation leads to a characteristic thermal relaxation length,

$$\rho=(2\kappa/3nkG\nu_{ei})^{1/2},$$

where τ_{ei} is replaced by $(1/G\nu_{ei})$ with $G=2m/M$ being twice the electron-to-ion mass ratio and ν_{ei} is the electron-ion collision frequency. Inserting the theoretical value of κ,[1] we get

$$\rho=\frac{5}{2}\left(\frac{3}{\pi}\right)^{1/2}\frac{\delta}{n\ln[(kT/e^2)^3/n]\sqrt{G}}\left(\frac{kT}{e^2}\right)^2,$$

where the factor δ is of the order of unity. Thus, for electron temperature $T\approx300$°K, and electron number density $n\approx10^{11}$ cm^{-3}, we have $\rho\approx4.5\times10^{-2}/\sqrt{G}$ cm. A small value of G is favorable in this regard and this prompts us to use as heavy a gas molecule as possible.

The condition (2) mentioned above demands that the ratio of the electron-molecule to electron-ion collision frequency ν_{em}/ν_{ei} be as small as possible and that the electron number density be large. The actual choice of gas to be used was dictated by a number of

* Research supported by Air Force Cambridge Research Laboratory, under contract AF 19(604)-7473.
[1] R. Landshoff, Phys. Rev. **76**, 904 (1949).
[2] L. Goldstein and T. Sekiguchi, Phys. Rev. **109**, 625 (1958).
[3] T. Sekiguchi and R. C. Herndon, Phys. Rev. **112**, 1 (1958).
[4] L. Landau, Physik Z. Sowjetunion **10**, 154 (1936).
[5] A. Dougal and L. Goldstein, Phys. Rev. **109**, 615 (1958).

considerations. In order to relate the present work to earlier work and, in particular, to make use of the recombination light from noble gas afterglow, we restricted our choice to noble gases. Helium is ruled out because it is too light.

The choice of the remaining noble gases, then, depends on the relative values of electron-molecule collision probability.[6] Since the electron-molecule collision cross sections of Kr and Xe are relatively large, a large value of ν_{ei}/ν_{em} requires a very high electron number density as well as a low electron temperature. Hence the choice is restricted to neon and argon. Neon was chosen because of the fact that earlier experiments were done in neon.[2,5] The ratio $\nu_{em}/\nu_{ei}\approx 0.07$ for electron densities $n\approx 10^{11}$ cm^{-3} in neon at a pressure of 5 mm Hg and electrons at a temperature of 300°K. Thus, under these conditions the plasma simulates an almost fully ionized gas. It should be noted that for electron temperatures of the order of 1000°K, the plasma would no longer have the properties of a fully ionized gas since $\nu_{em}\approx\nu_{ei}$. The analogy to a fully ionized gas fails in two respects due to the presence of neutral molecules. In the first, the ions are immersed in an effective heat bath of neutral molecules which fixes the ion temperature. This prevents the ions from contributing to the heat conduction process due to local heating by the electrons. In the second, the neutral molecules make possible the continuous conversion of atomic ions to molecular ions.

II. THEORY OF EXPERIMENT

II.1 Introduction

The experiment to be analyzed is one in which an idealized rectangular slab of plasma infinitely long is placed in a transverse magnetic field as shown in Fig. 1(b). Electrons in a localized volume of the plasma are uniformly heated by an electromagnetic wave of frequency 7500 Mc/sec. Conduction of the heat by the electron gas alone takes place, and the resulting thermal distribution of the electrons is measured by the "afterglow quenching" technique.[7] The frequency of the electromagnetic wave is so high that the temperature of the ions is unaffected.

The assumption of negligible charge concentration gradients across the plasma (y direction) may be justified by the magnetic field which inhibits diffusion to the sides of the plasma. Such arguments cannot be invoked for the flow parallel to the field. Here an estimate of the heat loss due to ambipolar diffusion has been shown to be small compared to those due to the temperature gradients.

In order to effectively compare the predictions of theory with experiment it is necessary to derive the usual heat equation for the electron gas based on conservation of energy and charge. We cannot derive the heat equation, however, until we make an assumption about either the local fields or the local currents. Due to the impressive success in the past of the ambipolar flow concept, we assume that it is effective in the present experiment. Further refinements of the experiment or of the theory may make this assumption untenable.

II.2 Relation of Thermomagnetic Coefficients to Landshoff's Calculation

Callen[8] has provided a convenient tabulation of thermomagnetic effects of a conducting medium in the following matrix form:

$$\begin{bmatrix} -\nabla_x\bar{\mu}/e \\ -\nabla_y\bar{\mu}/e \\ Q_x \\ Q_y \end{bmatrix} = \begin{bmatrix} \sigma_i^{-1} & HR_i & \alpha & -H\eta_i \\ -HR_i & \sigma_i^{-1} & H\eta_i & \alpha \\ \alpha T & -TH\eta_i & -\kappa_i & -H\kappa_i S \\ TH\eta_i & \alpha T & H\kappa_i S & -\kappa_i \end{bmatrix} \times \begin{bmatrix} j_x \\ j_y \\ \nabla_x T \\ \nabla_y T \end{bmatrix}, \tag{1}$$

for the transverse components in the x-y plane. In the z direction, that of the magnetic field H, the appropriate equations may be written

$$-\nabla_z\bar{\mu}/e=(j_z/\sigma_0)+\alpha_0\nabla_z T,$$
$$Q_z=\alpha_0 T j_z-\kappa_0\nabla_z T,$$

the subscript zero referring to zero magnetic field. The coefficients σ_i, R_i, κ_i, and η_i are the isothermal conductivity, Hall coefficient, thermal conductivity, and Nernst coefficient, respectively; α and S are the thermoelectric power and Leduc-Righi coefficient; $\bar{\mu}$ is the electrochemical potential and is equal to the sum $Ze\varphi+\mu$ of the electrical potential $Ze\varphi$ and chemical potential μ, where Z is the sign of the charge; $\mathbf{Q}$ is the heat flux and is to be thought of as the product of the absolute temperature and the entropy current; $\mathbf{j}$ is the electric current density.

We find it convenient to rewrite the equations in complex form,

$$-\frac{(\nabla_x+i\nabla_y)\bar{\mu}^{\pm}}{Z^{\pm}e}=\left(\frac{1}{\sigma_i^{\pm}}+iHR_i^{\pm}\right)(j_x^{\pm}+ij_y^{\pm}) +(\alpha^{\pm}+iH\eta_i^{\pm})(\nabla_x+i\nabla_y)T^{\pm}, \tag{2}$$

$$-\frac{\nabla_z\bar{\mu}^{\pm}}{Z^{\pm}e}=\frac{j_z^{\pm}}{\sigma_0^{\pm}}-\alpha_0^{\pm}\nabla_z T^{\pm},$$

$$Q_x^{\pm}+iQ_y^{\pm}=T^{\pm}(\alpha^{\pm}+iH\eta_i^{\pm})(j_x^{\pm}+ij_y^{\pm}) -\kappa_i^{\pm}(1+iHS^{\pm})(\nabla_x+i\nabla_y)T^{\pm}, \tag{3}$$

$$Q_z^{\pm}=T^{\pm}\alpha_0^{\pm}j_z^{\pm}-\kappa_0^{\pm}\nabla_z T^{\pm},$$

[6] A. V. Phelps, O. T. Fundingsland, and S. C. Brown, Phys. Rev. 84, 559 (1951).

[7] L. Goldstein, J. M. Anderson, and G. L. Clark, Phys. Rev. 90, 486 (1953).

[8] H. B. Callen, Phys. Rev. 85, 16 (1952).

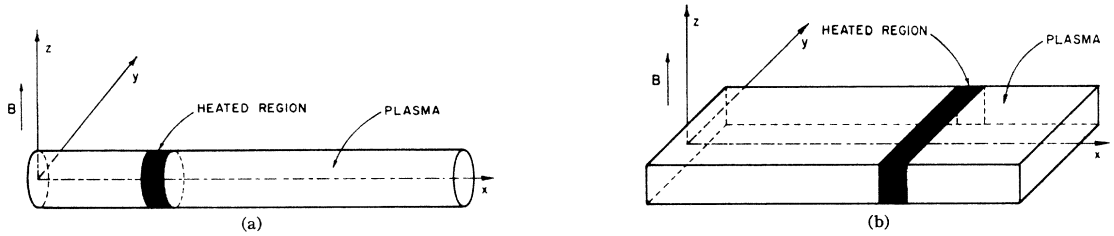

FIG. 1. The plasma column geometries. (a) Cylindrical geometry; (b) rectangular geometry.

where the superscripts + and − refer to the ion and electron species, respectively.

We shall next make use of the ambipolar flow assumption. We assume that $j_x^+ + ij_y^+ = -j_x^- - ij_y^- = -J_x^- - iJ_y^-$, and $j_z^+ = -j_z^- = -J_z^-$, where $\mathbf{J}^-$ is the electron ambipolar current. Then,

$$J_x^- + iJ_y^- = \frac{(\alpha^+ + iH\eta_i^+)(\nabla_x + i\nabla_y)T^+ - (\alpha^- + iH\eta_i^-)(\nabla_x + i\nabla_y)T^- + (\nabla_x + i\nabla_y)(\mu^+ + \mu^-)/e}{(1/\sigma_i^+) + (1/\sigma_i^-) - iH(R_i^+ + iR_i^-)}, \tag{4}$$

and

$$J_z^- = \frac{\alpha_0^+ \nabla_z T^+ - \alpha_0^- \nabla_z T^- + \nabla_z(\mu^+ + \mu^-)/e}{(1/\sigma_0^+) + (1/\sigma_0^-)}.$$

The energy conservation equation for the electrons is ordinarily derived from the Boltzmann equation.[9] In the absence of center-of-mass motion, the energy equation may be written

$$\frac{\partial(\frac{3}{2}n^- kT^-)}{\partial t} = -\nabla\cdot\mathbf{q}^- + \mathbf{j}^-\cdot\mathbf{E} + \int \tfrac{1}{2}mv^2\left(\frac{\partial f}{\partial t}\right)_{\text{coll}} d\mathbf{v}, \tag{5}$$

where $\frac{3}{2}kT^- = \langle\frac{1}{2}mv^2\rangle_{\text{av}}$, $\mathbf{q} = \langle\frac{1}{2}nmv^2\mathbf{v}\rangle_{\text{av}}$, and $\mathbf{E}$ is the electric field. Included in the last term, the collisional term, is the possible heating due to collisions with metastables, cooling due to collisions with other species, and cooling due to removal of electrons by recombination. The effect of collisions may be written in the form,

$$\int \tfrac{1}{2}mv^2\left(\frac{\partial f}{\partial t}\right)_{\text{coll}} d\mathbf{v} = -\left[\frac{\frac{3}{2}nk(T^- - T^+)}{\tau_{\text{ei}}}\right] + \tfrac{3}{2}kT_r\left(\frac{\partial n^-}{\partial t}\right)_r, \tag{6}$$

where the first term in (6) refers to electron-ion collisional cooling and the last term in (6) represents cooling due to recombination. The energy $\frac{3}{2}kT_r$ is that characteristic of a recombining electron, and is somewhat lower than the ambient electron energy $\frac{3}{2}kT^-$. From the electronic charge-conservation equation we are able to replace $\frac{3}{2}kT^-(\partial n^-/\partial t)$ in (5) by

$$\tfrac{3}{2}kT^-(\partial n^-/\partial t) = -\nabla\cdot(\tfrac{3}{2}kT^-/e)\mathbf{j} + \mathbf{j}\cdot\nabla(\tfrac{3}{2}kT^-/e) + \tfrac{3}{2}kT^-(\partial n^-/\partial t)_r. \tag{7}$$

The heat equation (5) can then be reformulated making use of (6) and (7) to give

$$\begin{aligned}\tfrac{3}{2}n^- k(\partial T^-/\partial t) = &-\nabla\cdot[\mathbf{q}^- + \tfrac{3}{2}(kT^-/e)\mathbf{j}^-] \\ &+ \mathbf{j}^-\cdot\nabla\tfrac{3}{2}(kT^-/e) + \mathbf{j}^-\cdot\mathbf{E} \\ &+ \tfrac{3}{2}n^- k(T^- - T^+)(1-\alpha n^-\tau_{\text{ei}})/\tau_{\text{ei}} \\ &+ \tfrac{3}{2}\alpha(n^-)^2 k(T^+ - T_r),\end{aligned} \tag{8}$$

where the second term on the right-hand side is the Thomson heating term and α is the electron-ion recombination coefficient. The last term in (8) is small and can be neglected. In our experiments, $\alpha n\tau_{\text{ei}} < 0.5$.

To complete the analysis, the connection between the previously defined heat fluxes $\mathbf{q}^-$ and $\mathbf{Q}^-$ is needed. Reference to a work on irreversible thermodynamics[10] provides the relation

$$\mathbf{q}^- = \mathbf{Q}^- - \mu^-\mathbf{j}^-/e. \tag{9}$$

Assuming that $\mu^- = kT\ln[nh^3/(2\pi mkT^-)^{3/2}]$ and assuming that $\nabla n^+ = \nabla n^- = \nabla T^+ = 0$, a rather straightforward analysis using Eqs. (3), (4), and (9) gives the result

$$\begin{aligned}\mathfrak{Q}_x + i\mathfrak{Q}_y &= q_x^- + iq_y^- + \tfrac{3}{2}(kT/e)(J_x^- + iJ_y^-) \\ &= -\left\{\kappa_i^-(1+iHS^-) + \frac{T^-[(\alpha^- + iH\eta^-) + (\frac{3}{2} - \mu^-/kT^-)k/e]^2}{(1/\sigma_i^+) + (1/\sigma_i^-) - iH(R_i^+ + R_i^-)}\right\}(\nabla_x + i\nabla_y)T^-,\end{aligned} \tag{10}$$

and

$$\mathfrak{Q}_z = q_z + \tfrac{3}{2}(kT^-/e)J_z^- = -\left\{\kappa_0^- + \frac{T^-[\alpha_0 + (\frac{3}{2} - \mu^-/kT^-)k/e]^2}{(1/\sigma_0^+) + (1/\sigma_0^-)}\right\}\nabla_z T^-.$$

[9] S. Chapman and T. G. Cowling, *The Mathematical Theory of Nonuniform Gases* (Cambridge University Press, New York, 1939), p. 135.

[10] S. R. De Groot, *Thermodynamics of Irreversible Processes* (North-Holland Publishing Company, Amsterdam, 1951).

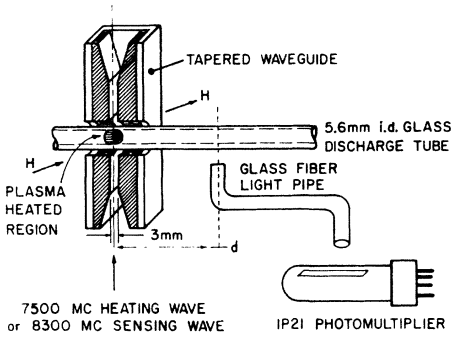

FIG. 2. Schematic diagrams showing tapered waveguide and light collecting method.

We note that (10) can be written in the form of a heat flux $\mathfrak{Q}=-\mathbf{K}\cdot\nabla T$, where $\mathbf{K}$ is the thermal conductivity tensor.

Landshoff has calculated the transport coefficients defined in Eq. (1) for a fully ionized gas in which electron-electron interactions are also taken into account. If we denote by $\tilde{\sigma}$, $\tilde{\tau}$, $\tilde{\mu}$, and $\tilde{K}$ the quantities denoted by σ, τ, μ, and K by Landshoff, his Eqs. (31) and (32) may be rewritten in the form

$$(\nabla_x+i\nabla_y)\bar{\mu}^-/e=[(j_x^-+ij_y^-)/\tilde{\sigma}] -\{[(\tfrac{5}{2}-\mu^-/kT^-)k/e]+\tilde{\tau}/\tilde{\sigma}\}(\nabla_x+i\nabla_y)T^-, \quad (11)$$

and

$$Q_x^-+iQ_y^-=-[(\tilde{\mu}/\tilde{\sigma})-\mu^-/e](j_x^-+ij_y^-) -(\tilde{K}-\tilde{\mu}\tilde{\tau}/\tilde{\sigma})(\nabla_x+i\nabla_y)T^-. \quad (12)$$

Comparison of (11) with (2) and of (12) with (3) shows that

$$(\tilde{\mu}/\tilde{\sigma}T^-)-\mu^-/eT^-=-\alpha^--iH\eta^-,$$

and the constitutive Onsager relation is

$$\tilde{\mu}/\tilde{\sigma}=(5kT^-/e)+\tilde{\tau}T^-/\tilde{\sigma}$$

between the Landshoff coefficients.

In terms of the Landshoff coefficients, the effective complex thermal conductivity $\kappa=\kappa_{xx}+i\kappa_{xy}$ as determined from Eq. (10) becomes

$$\kappa=\kappa_{xx}+i\kappa_{xy}=\tilde{K}-(\tilde{\mu}\tilde{\tau}/\tilde{\sigma}) +\frac{T^-[(\tilde{\tau}/\tilde{\sigma})+k/e]^2}{[(1/\tilde{\sigma})+(1/\sigma_i^+)-iHR_i^+]}. \quad (13)$$

Numerical estimates made in connection with our experiment indicate that the third, or ambipolar term, in Eq. (13) can be ignored. Therefore the appropriate thermal conductivity is the isothermal conductivity,

$$\kappa=\tilde{K}-\tilde{\mu}\tilde{\tau}/\tilde{\sigma}=\left(\frac{25nk^2T}{4m\nu}\right)A,$$

where

$$A=\left[\left(\frac{\Delta_{00}}{\Delta}\right)\left(\frac{\Delta_{11}}{\Delta}\right)-\left(\frac{\Delta_{01}}{\Delta}\right)^2\right]\Big/\left(\frac{\Delta_{00}}{\Delta}\right),$$

in Landshoff's notation. Additionally, the Joule and Thomson heating terms in (8) have been estimated and found to be negligible due to the weak ambipolar electron current $\mathbf{J}^-$. Consequently, we may write for the heat equation (8) the simplified equation

$$(\tfrac{3}{2}n^-k)\frac{\partial\theta}{\partial t}=\kappa_{xx}\left(\frac{\partial^2\theta}{\partial x^2}+\frac{\partial^2\theta}{\partial y^2}\right)+\left(\frac{\partial\kappa_{xx}}{\partial T^-}\right)\left[\left(\frac{\partial\theta}{\partial x}\right)^2+\left(\frac{\partial\theta}{\partial y}\right)^2\right] -\frac{3n^-k\theta(1-\alpha n\tau_{ei})}{2\tau_{ei}}, \quad (14)$$

where $\kappa_{xx}=\mathrm{Re}(\tilde{K}-\tilde{\mu}\tilde{\tau}/\tilde{\sigma})$ and $\theta=T^--T^+$. Terms in z have been neglected, since we heat the plasma uniformly in the z direction initially. Since the ambipolar effect is so small, the boundary is effectively insulating.

III. EXPERIMENTAL SETUP AND MEASUREMENTS

The relevant parameters connected with the measurement of the electronic heat conductivity are the electron number density n, the electron collision frequency ν, or the effective relaxation time τ, where $\tau=\tau_{ei}/(1-\alpha n\tau_{ei})$, and the temperature distribution in the electron gas.

The plasma under study is produced in a long thin glass discharge tube by a 3-kV dc pulse, 2 μsec long. Two discharge tube geometries are used, as shown in Fig. 1. In the circular cylindrical discharge tube (0.56-cm i.d. and 51 cm long) a stable and fairly uniform discharge was obtained by using a hot cathode and feeding the discharge pulse through an autotransformer. In the case of the rectangular discharge tube (0.75 cm $\times$1.75 cm, and 30 cm long) a fairly uniform discharge was obtained when the cathode was cold and grounded. In the cylindrical discharge tube the afterglow plasma lasted for $\approx$500 μsec whereas it was somewhat longer in the rectangular discharge tube. All measurements are made between 100 and 350 μsec in the neon (at 5 mm Hg) plasma afterglow after the initiation of the discharge pulse.

The present experimental setup is similar to earlier work.[2,3] In the case of the cylindrical discharge tube the plasma forms a post across the waveguide as shown in Fig. 2. As before parameters n and ν are determined by measuring the normalized microwave impedance of the plasma considered as a dielectric post,[11,2] traversing a WR137 waveguide. A probing 8300-Mc/sec frequency wave is used to measure n and ν. Proper account for the presence of magnetic field can easily be made as long as the electron cyclotron frequency is small compared to the microwave signal frequency. The above condition is not satisfied for the largest magnetic fields (1200 Oe) used in the experiment, since the cyclotron

[11] *Wave Guide Handbook*, Massachusetts Institute of Technology Radiation Laboratory Series No. 10 (McGraw-Hill Book Company, Inc., New York, 1957), p. 266.

frequency $f_H = 3.4 \times 10^9$ cps, and the signal frequency, $f = 8.3 \times 10^9$ cps. In this case errors of 30% in ν and 15% in n are expected.

Electron number densities ranging from 10^{11} to $5 \times 10^{12}/\text{cm}^3$ are readily measured. The electron collision frequency is determined in the range of 3×10^9 to 2×10^{10}/sec in the present experiment. Due to uncertainty in the exact diameter of a "uniform" plasma post the absolute value of the number density is rather difficult to determine. However, a reasonable estimate of relative variations of electron number density is obtained. The determination of electron collision frequency is insensitive to the assumed diameter of the plasma post. This has been checked against the measured energy relaxation time τ as determined by light intensity measurements. The two measurements agree within 20% of each other if it is assumed that the neon ions are mostly of the molecular type.

In the case of the rectangular discharge tube the microwave measurements of n and ν were not attempted because of the difficulties involved although it is by no means impossible. As discussed later, relative estimates of thermal conductivity can be made without making use of the explicit values of these parameters.

The waveguides (WR137) through which the discharge tubes pass are tapered in the middle as shown in Fig. 2. At appropriate times in the afterglow, a high-power ($\approx$100mW) microwave signal (7500 Mc/sec) is propagated along the waveguide in pulses of 10–30 μsec duration. This microwave signal selectively heats the electrons in a small, well-defined region of the long plasma column.

The phenomenon of "afterglow quenching"[7,2] is exploited for the measurement of the temperature distribution in the plasma column. The "steady-state" method[2] is used to measure the heat flow in the electron gas. From experimental evidence in this laboratory it is reasonable to assume that the electron temperature T^- will have decayed almost to the ion temperature T^+ at the time of measurement.

The afterglow light is monitored by an arrangement consisting of a suitable light pipe, a 1P21 photomultiplier tube and a dial indicator. The light pipe is made of 3-mm diameter Pyrex rod or by a number of 0.5-mm diameter quartz fibers assembled in a bundle. This arrangement limited the area of observation to 3 mm^2. The phenomenon of heat flow in the plasma column is studied by plotting the temperature profile with the help of the movable phototube assembly. Figure 3 shows typical afterglow light quenching phenomena, reflecting the electron temperature change due to the local heating. A set of such pictures as shown in Fig. 4 allows the evaluation of the space distribution of the electron temperature.

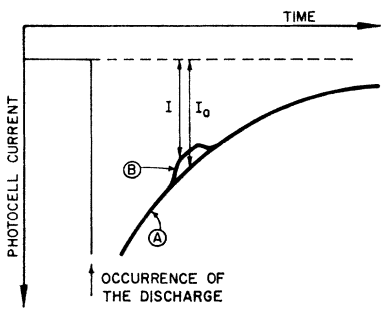

FIG. 3. The phenomenon of afterglow quenching; curve A shows the decay of the afterglow light and curve B shows the quenching of the light signal due to the local electron temperature rise. The relative temperature rise $(T^- - T^+)/T^+$ is given by $(I_0/I)^{2/3} - 1$.

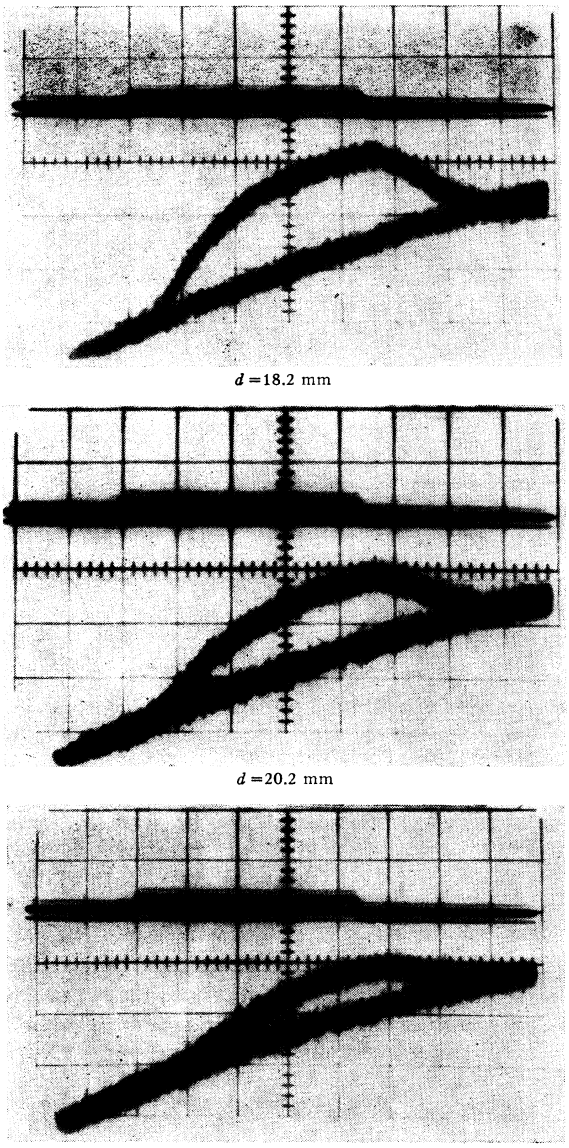

FIG. 4. Photographs of oscilloscope traces showing a typical sequence of quenched light signals at various distances d from the heated region for a cylindrical plasma. The discharge parameters are: Neon gas at 7 mm Hg, 200 μsec in the afterglow, $H = 660$ Oe, $n = 5.5 \times 10^{11}/\text{cm}^3$. The time scale is 5 μsec/cm.

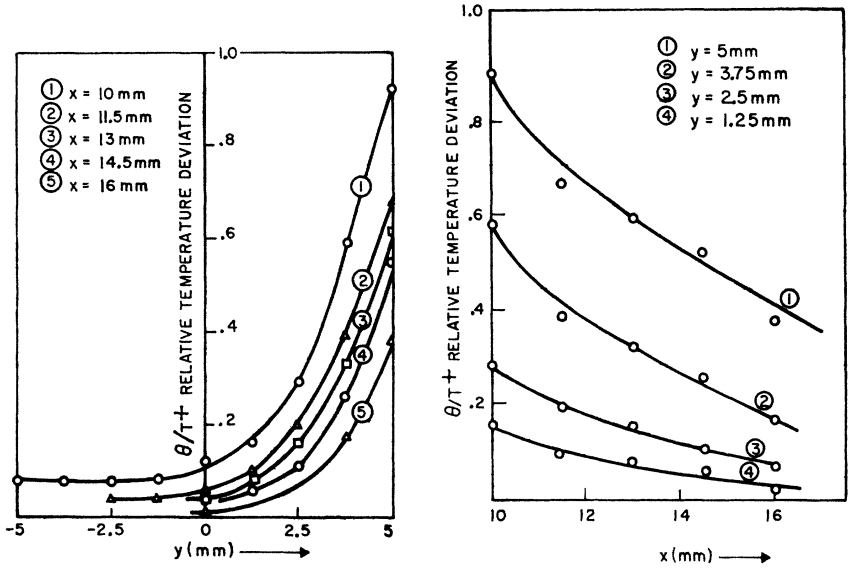

FIG. 5. The experimental temperature distribution in the rectangular plasma column. (a) Relative temperature variations as a function of y for various values of x; (b) relative temperature variation as a function of x for various values of y. ($\theta = T^- - T^+$.) Neon gas at 2.5 mm Hg, 90 μsec in the afterglow, $H = 600$ Oe.

When the magnetic field is perpendicular to the temperature gradient in the plasma, a nonuniform temperature distribution in the plane transverse to the magnetic field results. In the case of circular discharge tube, it is impossible to measure temperature distributions in the y direction (see Fig. 1). A rectangular discharge tube with the broader side transverse to the magnetic field and the heat flow is suitable for measurements of transverse temperature distributions in both the x and y directions.

The energy relaxation time τ is measured from the trailing edge of the decay of the quenched light signal. The electron temperature T^- decays to that of the ions T^+, once the heating is stopped. The time constant of this decay is the energy relaxation time. From Eq. (8),

$$\partial T^-/\partial t = -(T^- - T^+)(1-\alpha n\tau_{ei})/\tau_{ei} = -(T^- - T^+)/\tau,$$

where it has been assumed that the elastic electron-ion collisions and recombination are mainly responsible for the electron energy relaxation.

IV. EXPERIMENTAL RESULTS AND COMPARISON WITH THEORY

In this section we present the experimental results and compare them with theory. After presenting the data, we compare it with the theory by two methods; the first consists of a check of consistency with the heat equation and the second a comparison of our thermal conductivity estimates with those of Landshoff.[1]

As mentioned earlier, it has been found possible to measure the transverse and longitudinal temperature profile in the rectangular tube. An example of the steady-state transverse temperature distribution for various values of x is shown in Fig. 5(a) for neon at a pressure of 2.5 mm Hg and a magnetic field of 600 Oe. The corresponding longitudinal distribution is given in Fig. 5(b) with y as the parameter. It is clear that the heat is concentrated toward large values of y. This is consistent with the electrodynamic force on the electron gas in which heat is carried.

It has been found that in the steady state, the temperature distribution is essentially exponential in both the transverse and longitudinal directions, as shown in Figs. 6(a) and 6(b). Thus, the temperature distribution shows similar characteristics to that already discussed in zero magnetic field.[2]

We propose testing the experimental data in the following way. The thermal conductivity can be written as

$$\kappa_{xx} = (25nk^2T^-/4m\nu)A(\omega_H/\nu),$$

where ν is a parameter defined by Landshoff[1] and is equal to the electron-ion collision frequency calculated from Landau[4] when Landau's cutoff procedure is followed. We note that the heat equation, Eq. (14), can be written as

$$A\left(\frac{\partial^2\theta}{\partial x^2}+\frac{\partial^2\theta}{\partial y^2}\right)+\left[(5A/2)+(3\omega_H/2\nu)\frac{\partial A}{\partial(\omega_H/\nu)}\right]\times\left[\left(\frac{\partial\theta}{\partial x}\right)^2+\left(\frac{\partial\theta}{\partial y}\right)^2\right]\Big/T^- = 6m\nu\theta(1-\alpha n\tau_{ei})/25kT^-\tau_{ei}, \quad (15)$$

in which ν was assumed to be proportional to $T^{-3/2}$. As can be seen in Figs. 6(a) and 6(b) the temperature distribution can be expressed as

$$\theta(x,y) \propto \exp[-(x/\rho_x)-(y/\rho_y)].$$

We can perform two tests on this data; (a) test how

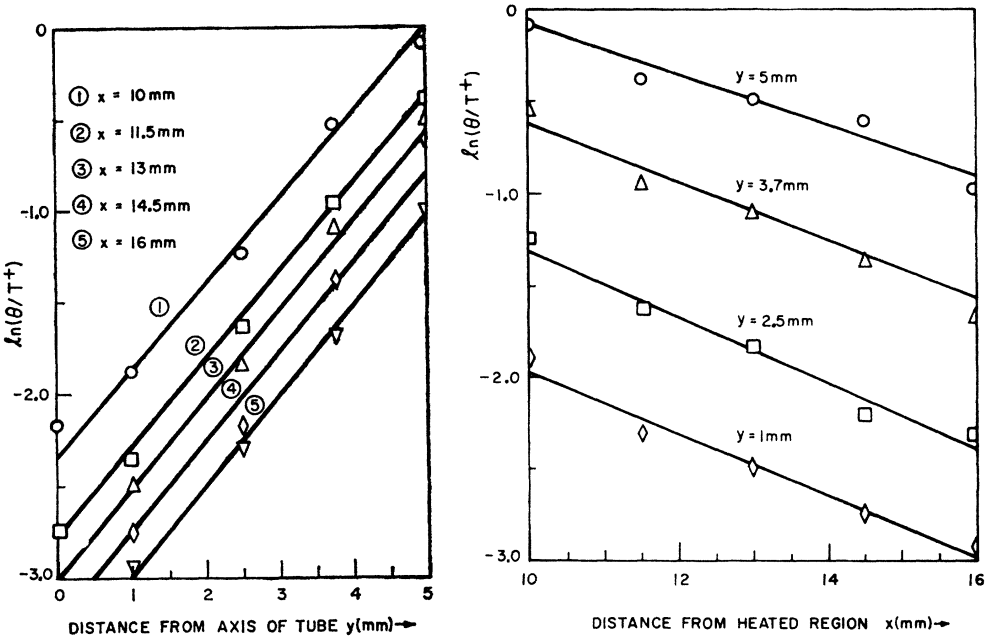

(a) (b)

FIG. 6. Same data as in Fig. 5 showing the exponential character of the temperature distribution.

well it satisfies the heat equation, and (b) test the boundary condition, $\mathfrak{Q}_y=0$, at the wall.

We may test the heat equation (15) by introducing the data for $\rho_x(\omega_H/\nu)$ and $\rho_y(\omega_H/\nu)$ into (15) and, letting $1/\rho^2=(1/\rho_x^2)+(1/\rho_y^2)$, consider the equation,

$$A\left\{1+\left[5+3\frac{\partial \ln A}{\partial \ln(\omega_H/\nu)}\right]\frac{\theta}{2T^-}\right\}=\left(\frac{6m}{25GkT^-\tau}\right)[(1/\tau)+\alpha n]\rho^2, \quad (16)$$

where $\nu=1/G\tau_{ei}$ has been assumed, and using the exponential space dependence of $\theta(x,y)$. The results of comparing both sides of Eq. (16) using the experimentally determined values of ρ_x, ρ_y, and τ_{ei} are shown in Table I. Figure 7 shows these quantities as a function of ω_H/ν. In Table I and Fig. 4, α was assumed to be 2×10^{-7} cm^3-sec^{-1} and n to be 10^{11} cm^{-3}. From Eq. (10) and the definition of κ, the transverse thermal current is given by

$$\mathfrak{Q}_y=-\kappa_{xy}(\partial\theta/\partial x)-\kappa_{xx}(\partial\theta/\partial y). \quad (17)$$

Assuming the exponential variation of $\theta(x,y)$, we show in Table II that $\mathfrak{Q}_y\approx0$, since $\rho_x/\rho_y\approx-\kappa_{xy}/\kappa_{xx}$. In addition, the calculated ratio of $\mathfrak{Q}_y/\mathfrak{Q}_x$ is also given.

In order to estimate the magnitude of the thermal conductivity tensor, we propose now to analyze the experiment from the point of view of a simplified heat equation, neglecting the temperature dependence of the thermal conductivity term. This approximation is valid for very small temperature deviations $\theta/T^-\ll1$. Equation (14) then becomes (in the steady state)

$$(\partial^2\theta/\partial x^2)+(\partial^2\theta/\partial y^2)=\theta/\rho_{xx}^2, \quad (18)$$

where $\rho_{xx}^2=2\kappa_{xx}\tau_{ei}/3nk(1-\alpha n\tau_{ei})$ is the characteristic length associated with the heat propagation.

The boundary conditions are the following:

(i) The temperature deviation θ is zero for $x=\infty$.
(ii) θ is constant, in the heated region.
(iii) The heat flow is zero at the boundaries.

As seen above the experimental temperature distribution suggests a solution of the form,

$$\theta(x,y)=\theta_0\exp[-(x/\rho_x)-y/\rho_y]. \quad (19)$$

It is seen immediately that such a solution will satisfy Eq. (18) if

$$1/\rho^2=(1/\rho_x^2)+1/\rho_y^2=1/\rho_{xx}^2. \quad (20)$$

This solution does not give a constant temperature

TABLE I. Comparison of the two sides of Eq. (16) as a function of ω_H/ν. The left-hand side, calculated from theory, is given in column 2. Column 3 is the right-hand side representing the data.

ω_H/ν	$A\left[1+\left(5+3\frac{\partial \ln A}{\partial \ln(\omega_H/\nu)}\right)\frac{\theta}{2T^-}\right]$ Assuming $\theta/T^-=0.6$ $T^-=750$°K; $T^+=300$°K	$6m\nu\rho^2/25\tau kT^-$ Assuming $\alpha n=2\times10^4$ sec^{-1}
0.0	1.27	2.55
0.2	1.05	1.89
0.5	0.49	0.695
1.0	0.21	0.205
2.0	0.092	0.045
4.0	0.037	0.016

TABLE II. Test of the assumption of zero transverse heat current density as predicted by Eq. (21). Column 4, the ratio of measured relaxation distances is to be compared with the theoretical ratio of thermal conductivities in column 7, obtained from columns 5 and 6. Column 8 gives an estimate of the relative magnitude of the transverse heat current density.

ω_H/ν	ρ_x	ρ_y	ρ_y/ρ_x	$4m\nu\kappa_{xx}/25nk^2T^-$	$4m\nu\kappa_{xy}/25nk^2T^-$	$-\kappa_{xx}/\kappa_{xy}$	$\mathfrak{Q}_y/\mathfrak{Q}_x$
0.0	0.86	∞	∞	0.5077	0	∞	...
0.2	0.86	...	...	0.4440	−0.1598	2.8	...
0.5	0.85	0.84	0.99	0.2751	−0.2356	1.17	0.07
1.0	0.83	0.44	0.53	0.1356	−0.1977	0.69	0.04
2.0	0.78	0.24	0.31	0.06198	−0.1279	0.48	0.11
4.0	0.65	0.16	0.25	0.02792	−0.07951	0.35	0.06

distribution in the heated region as required by condition (ii). In this region and close to it the complete solution evidently includes other terms which decay rapidly with x leaving only the term in Eq. (19) in the region of observation. Equation (19) satisfies the condition (i). For condition (iii) we have from Eq. (17) at the walls,

$$(\mathfrak{Q}_y)_{\text{wall}}=[(\kappa_{xy}/\rho_x)+\kappa_{xx}/\rho_y]\theta_{\text{wall}}=0.$$

Therefore,

$$\rho_x/\rho_y=-\kappa_{xy}/\kappa_{xx}. \tag{21}$$

From (20) and (21) we now have means of approximating κ_{xy} and κ_{xx} from ρ_x, ρ_y, τ_{ei}, and n, namely,

$$\begin{aligned}\kappa_{xx}&=3nk\rho^2(1-\alpha n\tau_{ei})/2\tau_{ei},\\ \kappa_{xy}&=-3nk\rho^2(1-\alpha n\tau_{ei})\rho_x/2\tau_{ei}\rho_y.\end{aligned} \tag{22}$$

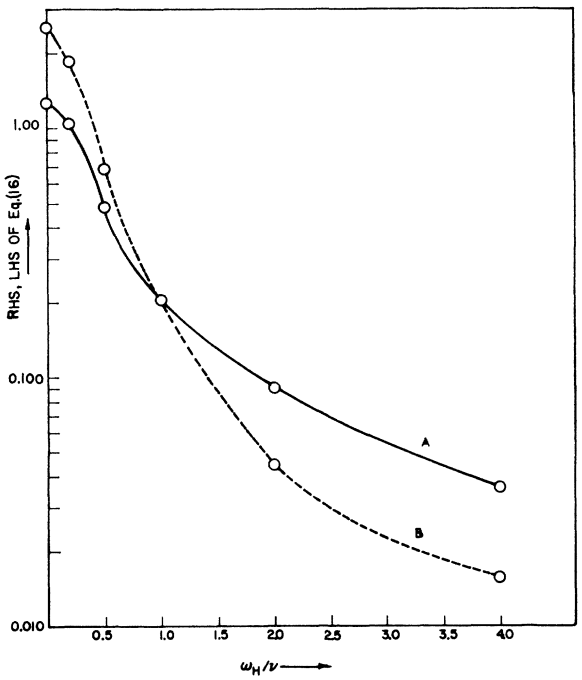

FIG. 7. Comparison of theory with experiment as a function of ω_H/ν by means of the heat equation as given by Eq. (16). The left-hand side is plotted as curve A and represents the theory. Curve B represents the experimental data substituted into the right-hand side of the equation. In curve A, θ/T^- is assumed to be 0.6, and αn to be 2×10^4 sec^{-1}.

It is expected that in the circular tube geometry a similar distribution is set up, at least in the x direction. Therefore the temperature averaged over the circular cross section would have the form

$$\langle\theta(x)\rangle_{\text{av}}=\langle\theta_0\rangle_{\text{av}}\exp(-x/\rho_x).$$

As shown in Appendix I the heat equation in one dimension leads to

$$\rho_x^2=2\tau_{ei}\kappa_{xx}/3nk(1-\alpha n\tau_{ei}), \tag{23}$$

where τ_{ei}, κ_{xx}, and n are averaged over the cross section of the discharge tube.

V. DISCUSSION OF RESULTS

A. Circular Tube

ρ_y could not be measured in this geometry because the transverse dimensions were too small and because of its circular cross section. However, n and ν were measured by microwave technique and τ_{ei} was measured using afterglow quenching.

From the formulation of the theory[1] the theoretical parameter of interest is the ratio of the cyclotron frequency to the electron-ion collision frequency (ω_H/ν). It was found impractical to vary the magnetic field in order to study the variation of the thermal conductivity with ω_H/ν. The magnetic field affects the initial discharge making it difficult to compare data taken at two different magnetic fields. This is due in part to the plasma post diameter change with magnetic field which renders difficult any comparison of microwave measurements. This is the reason why, in these measurements, it was found much easier to vary the collision frequency ν instead of the cyclotron frequency ω_H. This was done by keeping the magnetic field constant and making measurements at different times in the afterglow. The collision frequency then varies through its dependence on the number density and temperature of the electrons. However, only relative measurements can be made in this fashion. The heat conductivities measured at various times in the afterglow were always compared to the one measured at the earliest time in the afterglow (where ω_H/ν is the smallest).

If measurements of the quantities in Eq. (23) are made at the different times t_1 and t_2 in the afterglow, then the ratio of the thermal conductivities may be

TABLE III. Determination of the relative thermal conductivity in the cylindrical discharge tube $H=1125$ Oes, neon, 7.7 mm Hg.

Time in afterglow t (μsec)	Electron number density n (10^{12} cm^{-3})	Electron collision frequency ν (10^{10} sec^{-1})	Relaxation distance ρ_x (cm)	Measured relaxation time τ (μsec)	ω_H/ν	ν_{100}/ν[a]	$\left[\frac{A(1.56)}{A(\omega_H/\nu)}\right]_{\text{exp}}$	$\left[\frac{A(1.56)}{(\omega_H/\nu)A}\right]_{\text{theory}}$
100	1.615	1.41	0.63	2.05	1.56	1	1	1
125	1.185	1.205	...	...	...	...	...	...
150	0.904	1.042	0.75	3.15	1.93	1.235	1.05	1.26
175	0.680	0.935	...	...	...	...	...	...
200	0.511	0.861	0.94	7.1	2.56	1.639	1.65	1.71
225	0.389	0.788	...	...	...	...	...	...
250	0.311	0.679	0.95	9.5	3.24	2.08	2.33	2.230
300	0.209	0.297	1.14	11.3	4.25	2.74	2.31	3.180

[a] ν_{100} corresponds to ν at 100 μsec in the afterglow.

written

$$\frac{\kappa_{xx}(\omega_H(1)/\nu(1),T_1^-)}{\kappa_{xx}(\omega_H(2)/\nu(2),T_2^-)}=\frac{n_1\tau_2}{n_2\tau_1}\left(\frac{\rho_{x1}}{\rho_{x2}}\right)^2. \quad (24)$$

In order to compare such experimental ratios with theory, we consider the ratio

$$\frac{\kappa_{xx}(\omega_H(1)/\nu(1),T_1^-)}{\kappa_{xx}(\omega_H(2)/\nu(2),T_2^-)}=\frac{n_1T_1^-\nu_2A(\omega_H(1)/\nu(1))}{n_2T_2^-\nu_1A(\omega_H(2)/\nu(2))}. \quad (25)$$

Equating (24) and (25), we obtain

$$\frac{A(\omega_H(1)/\nu(1))}{A(\omega_H(2)/\nu(2))}=(\rho_{x1}/\rho_{x2})^2(\nu_1/\nu_2)^{5/3}(n_2/n_1)^{2/3}(\tau_2/\tau_1) \quad (26)$$

for the ratio of the ω_H/ν dependent parts, using $T\propto(n/\nu)^{2/3}$. A typical set of parameters are shown in Table III. They are compared with theory in Fig. 8.

B. Rectangular Tube

In this geometry the electron number density and collision frequency were not measured by the microwave interaction method. The collision frequency ν_{ei} was deduced from the energy relaxation time (τ_{ei}) measured by the afterglow quenching method using $\nu_{ei}=1/G\tau_{ei}$ with $G=3.7\times10^{-5}$ for the neon molecular ions.[12]

Relative variations of the number density were deduced from relative values of the relaxation time, since it depends on number density and temperature as

$$\tau_{ei}\propto\frac{(T^-)^{3/2}}{n\ln[(kT^-/e^2)^3/n]}. \quad (27)$$

As mentioned before, it was found desirable to keep H fixed while varying ν in the circular tube experiments. Because n could not be measured in the rectangular tube, it was decided to do all experiments at the same time in the afterglow and vary H. In this way, effects due to a change in n would be minimized, although the discharge may have varied slightly due to the magnetic field. For each value of the magnetic field ρ_x, ρ_y, and τ_{ei} were measured. It was then assumed that the equilibrium temperature of the electrons was not affected by the magnetic field so that variations of τ_{ei} which occur at a given time in the afterglow due to the magnetic field were entirely to be attributed to variations in number density of the electrons.

Some difficulty was encountered in obtaining a reasonably uniform number density in the cross section of the tube. In the presence of the magnetic field the discharge current through the tube would take distorted paths and be projected towards one wall by the $\mathbf{J}\times\mathbf{B}$ force. The nonuniformity thus created would decay by diffusion and at the time in the afterglow where the measurements were made, the uniformity was already much improved. It was further con-

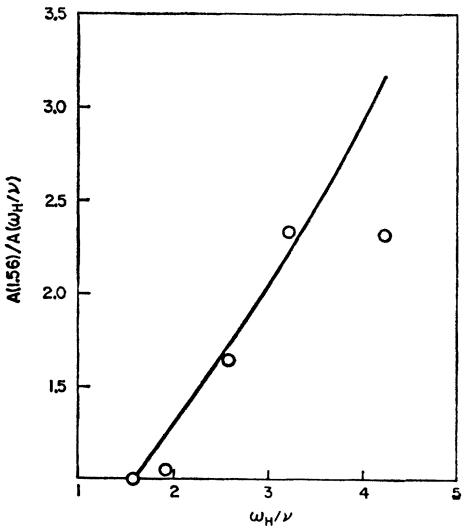

FIG. 8. The ratio $A(1.56)/A(\omega_H/\nu)$ (neglecting the temperature dependence of κ_{xx}/κ_0) for the cylindrical plasma as a function of ω_H/ν. The experimental points (○) refer to neon afterglow plasma at 7.7 mm of Hg with $H=1125$ Oe. The solid line is the theoretical curve.

[12] ν_{ei} values were deduced from $\tau=\tau_{ei}/(1-\alpha n\tau_{ei})$ since $\alpha n\tau_{ei}$ was small enough to be ignored.

TABLE IV. Experimental values of κ_{xx}, neglecting its temperature variation.

H (Oe)	ρ_x (mm)	ρ_y (mm)	τ (μsec)	$\nu_{ei}=1/G\tau_{ei}$ (10^9 sec^{-1})	ω_H/ν	$\kappa_{xy}/\kappa_{xx}=\rho_x/\rho_y$	κ_{xx}/κ_0
0	8.5	∞	5.2	8.4	0	0	1.00
160	8.5	8.9	6.4	6.5	0.43	0.96	0.35
260	8.65	5.7	7.5	5.7	0.81	1.5	0.15
360	7.75	3.56	8.3	5.2	1.2	2.18	0.056
460	6.7	2.46	11.0	4.1	2.0	2.73	0.0145
560	6.7	2.06	11.6	3.9	2.5	3.27	0.010
760	7.5	1.78	11.5	4.0	3.4	4.20	0.0085
860	6.0	1.65	11.0	4.1	3.7	3.64	0.0080
960	7.2	1.65	12.4	3.7	4.6	4.35	0.0064
1060	6.0	1.53	12.0	3.8	4.8	3.92	0.0057

siderably improved by reducing the gas pressure to 2.5 mm and thus enhancing the diffusion in the cross section. The electron number density was monitored in the cross section in the y direction by studying the variation of the afterglow light intensity (assumed proportional to n^2).

Very approximate relative values of κ_{xx} are obtained by reference to Eq. (24). Since it has been assumed that the ambient electron temperature does not depend on magnetic field, we may approximate the ratios of electron number density in Eq. (24) by the reciprocal ratios of relaxation time from Eq. (27), obtaining

$$\kappa_{xx}(1)/\kappa_{xx}(2)=(\rho_1\tau_2/\rho_2\tau_1)^2,$$

from which the relative variations of κ_{xx} may be plotted. This has been done in Figs. 9 and 10 from data given in Table IV. In Figs. 9 and 10 the theory developed earlier in this paper is compared with the experimental points.

VI. CONCLUSIONS

The thermal distribution in a locally heated magnetoplasma has been determined and the measurements have been compared with Landshoff's[1] calculations for a fully ionized magnetoplasma.

Two methods have been presented for interpreting the data. In the first we have attempted to fit the heat equation using the experimental temperature distribution. There we found order of magnitude agreement with theory, with, however a progressive deviation toward lower ω_H/ν values. The second method was to ignore the temperature dependence of the thermal conductivity tensor which makes it possible to estimate an experimental value of the thermal conductivity tensor. One of the benefits of the latter analysis is to

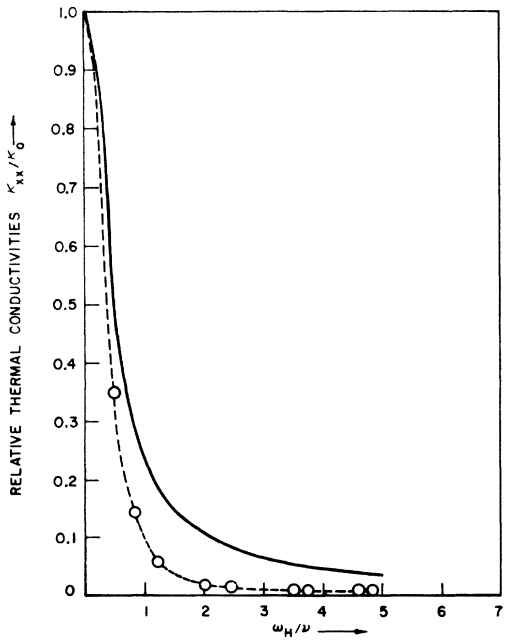

FIG. 9. Relative thermal conductivity κ_{xx}/κ_0 for the rectangular plasma geometry (neglecting the temperature dependence of κ_{xx}/κ_0) as a function of ω_H/ν. The experimental curve (- O - O -) refers to a neon plasma at 2.5 mm of Hg, 200 μsec in the afterglow.

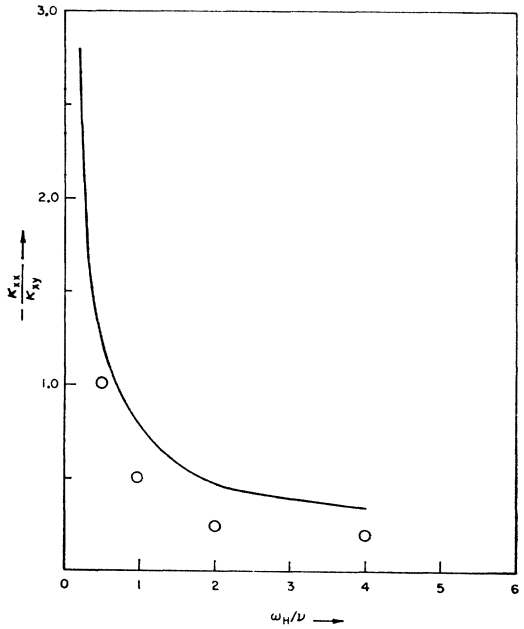

FIG. 10. Test of conditions of zero transverse heat flow $\Omega_y=0$. Solid line shows $-\kappa_{xx}/\kappa_{xy}$ as a function of ω_H/ν. The experimental points are the ratio ρ_y/ρ_x [cf. Eq. (21)] in neon at 2.5 mm Hg, 200 μsec in the afterglow.

permit a comparison of experiments done both on cylindrical and rectangular discharge geometries. It was found that the thermal conductivity determined in the cylindrical tube displays a variation very similar to that found in the rectangular tube. This confirms the validity of the use of light measurements alone in the study of thermal transport processes.

ACKNOWLEDGMENTS

The authors thank Dr. L. Goldstein for suggesting this problem and for his advice and encouragement during the course of the research.

APPENDIX I

Derivation of the Heat Equation—Circular Tube

Measurements made on the circular discharge tube are one dimensional so it is necessary to derive a one-dimensional heat equation with which to interpret the data.

This can be done by considering a short cylindrical section of the discharge tube and integrating the energy continuity equation over the volume. The resulting equation in the steady state is then, from Eq. (8)

$$\int \Omega_x d\Sigma_{x+dx} - \int \Omega_x d\Sigma_x = -\frac{3}{2}\int\left[nkT^- \frac{(1-\alpha n\tau_{ei})}{\tau_{ei}}\right]dV,$$

if the surface heat currents are assumed to vanish, the Joule and Thomson heating is negligible, and Ω_x is given by Eq. (10). The integration over the ends is indicated by the subscripts on the surface element. In order to evaluate $\int \Omega_x d\Sigma_x$ we make use of the fact that the temperature distribution $\theta = T^- - T^+$ is of the form $\exp[-(x/\rho_x) - y/\rho_y]$ even in circular geometry. Then it is readily shown that,

$$\int \Omega_x d\Sigma_x \propto (1-\rho_x\rho_y\langle\kappa_{xy}\rangle/\langle\kappa_{xx}\rangle),$$

where $\langle\ \rangle$ means averaged over the circular cross section. From measurements, $\rho_x\rho_y \approx 1/25$ and $\langle\kappa_{xy}\rangle/\langle\kappa_{xx}\rangle \leqslant 4$. Hence an error of the order of 10% is made in neglecting the second term. If we do so, the resulting one-dimensional heat equation becomes

$$\frac{\partial}{\partial x}\left\langle \kappa_{xx}\frac{\partial\theta}{\partial x}\right\rangle = \frac{3}{2}\left\langle nk\theta\frac{(1-\alpha n\tau_{ei})}{\tau_{ei}}\right\rangle,$$

averaged over the circular cross section.

A further simplification can be obtained under certain conditions. We have

$$\frac{\partial}{\partial x}\left\langle \kappa_{xx}\frac{\partial\theta}{\partial x}\right\rangle = \left\langle \kappa_{xx}\frac{\partial^2\theta}{\partial x^2}\right\rangle + \left\langle \frac{\partial\kappa_{xx}}{\partial T^-}\frac{\partial\theta}{\partial x}\right\rangle^2$$

$$= \left\langle \kappa_{xx}\frac{\partial^2\theta}{\partial x^2}\left\{1+\left[\left(\frac{\partial\theta}{\partial x}\right)^2 \Big/ \frac{\partial^2\theta}{\partial x^2}\right]\frac{d\ln\kappa_{xx}}{dT^-}\right\}\right\rangle.$$

When $\theta \propto \exp(-x/\rho_x)$, the second term is of order $\theta d\ln\kappa_{xx}/dT^-$ which produces an error not in excess of 10% when $\theta/T^- \ll 0.04$. This corresponds to a value of $I_0/I < 0.0084$.

Under these conditions we can write

$$\langle\kappa_{xx}\rangle\langle\partial^2\theta/\partial x^2\rangle \approx \tfrac{3}{2}\langle n\rangle k\langle\theta\rangle\langle 1-\alpha n\tau_{ei}\rangle/\langle\tau_{ei}\rangle.$$

If $\theta \propto \exp(-x/\rho_x)$, then $\rho_x^2 = \frac{2}{3}\langle\kappa_{xx}\rangle\langle\tau_{ei}\rangle/\langle n\rangle k\langle 1-\alpha n\tau_{ei}\rangle$ and $\langle\kappa_{xx}\rangle$ may be determined.

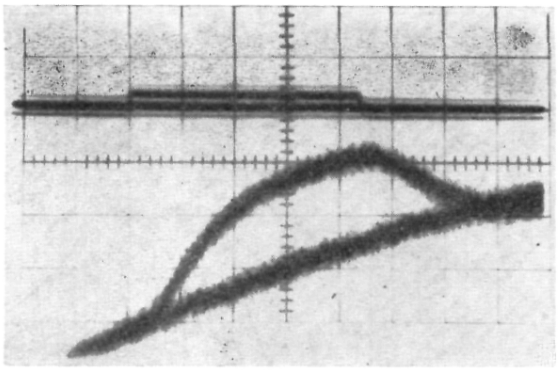

$d = 18.2$ mm

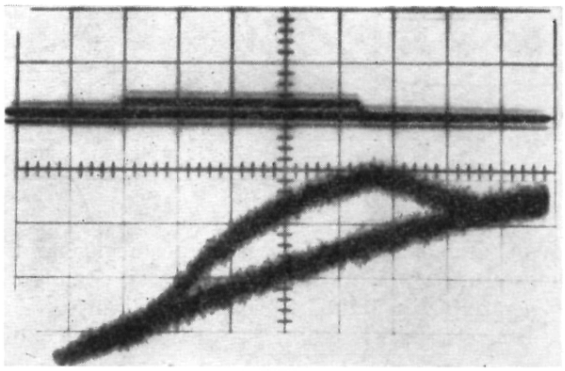

$d = 20.2$ mm

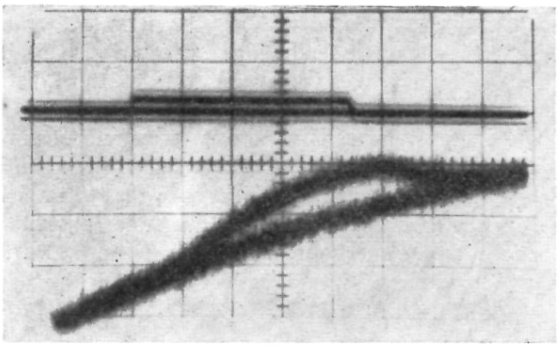

$d = 22.7$ mm

FIG. 4. Photographs of oscilloscope traces showing a typical sequence of quenched light signals at various distances d from the heated region for a cylindrical plasma. The discharge parameters are: Neon gas at 7 mm Hg, 200 μsec in the afterglow, $H = 660$ Oe, $n = 5.5 \times 10^{11}/\text{cm}^3$. The time scale is 5 μsec/cm.